THE ASTROPHYSICAL JOURNAL, 338:812–823, 1989 March 15

THE ULTRAVIOLET SPECTRUM OF AN OXYGEN-RICH SUPERNOVA REMNANT IN THE SMALL MAGELLANIC CLOUD

WILLIAM P. BLAIR[1]
The Johns Hopkins University
JOHN C. RAYMOND[1]
Harvard-Smithsonian Center for Astrophysics
AND
JOHN DANZIGER[1] AND FRANCESCA MATTEUCCI[1]
European Southern Observatory
Received 1988 July 11; accepted 1988 August 16

ABSTRACT

We present ultraviolet and optical spectral data for the oxygen-rich supernova remnant 1E 0102−7219 in the Small Magellanic Cloud. The ultraviolet data were obtained with the *IUE* satellite and are the first data to seriously constrain the ultraviolet emission from an oxygen-rich remnant. Emission lines of O I, [O II], O III], O IV], C III], C IV, [Ne IV], and Mg II have been unambiguously detected in the UV. The presence of O I recombination lines in the UV and optical permits a scaling of relative line intensities for comparison with models. We have calculated shock models for material with abundances appropriate to massive stellar ejecta and find a number of differences between these models and the observations. The UV lines are observed to be weaker relative to optical lines than expected from the models, and values of certain ratios, such as C IV λ1550/C III λ1909, are difficult to explain. We have also calculated models of photoionization by the remnant's X-ray emission, and these provide a better qualitative match to the observed spectra, although a combination of shock heating and photoionization may be necessary to explain all of the relative line intensities. We derive approximate abundances in the ejecta and discuss the implications these have for the precursor star.

Subject headings: galaxies: Magellanic Clouds — nebulae: abundances — nebulae: individual (1E 0102−7219) — nebulae: supernova remnants — ultraviolet: spectra

I. INTRODUCTION

The supernova remnant (SNR) 1E 0102.2−7219 was first identified in the *Einstein* X-ray survey of the Small Magellanic Cloud (SMC) by Seward and Mitchell (1981). Measurements with the Imaging Proportional Counter on *Einstein* show the object to be the second brightest X-ray source in the SMC and to have a relatively soft X-ray spectrum, similar to SNRs in our Galaxy and the Large Magellanic Cloud (LMC). However, it was clear even from the survey results that this object was not "typical." The IPC count rate was ≥ 10 times that of the next brightest SMC remnant.

Optical emission from 1E 0102.2−7219 was discovered by Dopita, Tuohy, and Mathewson (1981) using narrow band imaging. The SNR was identified with a faint ring of filaments $\sim 24''$ in diameter visible only in the light of [O III] λ5007, adjacent to the N67A. Comparison to existing radio data indicated that confusion with thermal emission had prevented the source from being identified as nonthermal, but that a radio source was present at the position of the SNR. The calibrated images revealed a ratio of [O III] λ5007/Hβ ≥ 60 for the ring of filaments. At a distance of 59 kpc for the SMC, the diameter of the [O III] ring is 6.9 pc.

The spectroscopic peculiarities of the SNR were demonstrated by Tuohy and Dopita (1983): spectra of individual knots showed strong lines of oxygen and neon, but nothing else. Velocity mapping indicated an overall expansion velocity of ~ 6500 km s^{-1}, perhaps distributed in a twisted ring morphology. Although Tuohy and Dopita claim an age of ~ 1000 yr, undecelerated expansion at ~ 3250 km s^{-1} implies an expansion age of 2150 yr. These characteristics clearly establish this remnant as a member of the class of oxygen-rich SNRs, which includes such objects as N132D and 0540−69.3 in the LMC (Lasker 1980; Mathewson *et al.* 1980), Cas A and G292.0+1.8 in our Galaxy (Chevalier and Kirshner 1978, 1979; Goss *et al.* 1979; Murdin and Clark 1979), and the powerful young SNR in the irregular galaxy NGC 4449 (Blair, Kirshner, and Winkler 1983). More recently, some knots dominated by oxygen emission have been identified in the Galactic remnant Puppis A (Winkler and Kirshner 1985), although this SNR is thought to be considerably older than the other members of the class.

Objects with inferred large overabundances of such elements as oxygen, neon, sulfur, etc., are thought to represent the explosions of massive (Population I) stars. Nuclear burning in the progenitor stars had progressed to or perhaps even beyond the oxygen-burning stage when the SN explosion took place. With the exception of Puppis A, the SNRs are all young (≤ 2500 yr), show high-velocity material ($\Delta v \geq 2000$ km s^{-1}), and contain some optical knots or filaments whose spectra are dominated by oxygen emission lines (hence, the class name "oxygen-rich" remnants). Since the X-ray emissivity depends on n_e^2 and is also a function of heavy element abundances (cf. Raymond and Smith 1977; Long, Dopita, and Tuohy 1982), these young, metal-rich SNRs also tend to be strong soft X-ray sources. 1E 0101.2−7219 meets all of these criteria. A summary of the

[1] Guest Observer with the *International Ultraviolet Explorer* satellite, which is jointly operated by the U.S. National Aeronautics and Space Administration, the Science Research Council of the UK, and the European Space Agency.

TABLE 1

CHARACTERISTICS OF 1E 0102.2−7219

Characteristic	Value	References
Distance	59 kpc	1
Position (1950)	$01^h02^m25^s.2$, $-72°18'04''.6$	2, 3
SNR diameter:		
Ring	$24'' = 6.9$ pc	2
Annulus	$40'' = 11.5$ pc	4
Velocities:		
Range	-2500 to $+4000$ km s^{-1}	4
Total	~ 6500 km s^{-1}	4
SNR age	~ 2150 yr	2, 3
X-ray luminosity (0.2–2 keV)	1.5×10^{37} ergs s^{-1}	5
T_e[O III]	~ 27000 K	6
N_e	≤ 100 cm^{-3}:	7

REFERENCES.—(1) McNamara and Feltz 1980; (2) Dopita, Tuohy, and Mathewson 1981; (3) Revised, this paper; (4) Tuohy and Dopita 1983; (5) Seward and Mitchell 1981, corrected to $D = 59$ kpc; (6) Using global spectrum of Dopita and Tuohy 1984 with [O III] atomic parameters from Osterbrock 1974; (7) Dopita and Tuohy 1984.

measured or inferred characteristics of this SNR is given in Table 1.

One of the difficulties in interpreting optical spectra of oxygen-rich SNRs is that there simply are not very many emission lines with which to constrain the physical conditions in the emitting material. Some elements such as carbon, silicon, and magnesium have no strong lines in the optical and their abundances are unconstrained by optical spectra. The ultraviolet region contains strong lines of these elements as well as oxygen and can be used to determine the relative abundances for comparison with nucleosynthesis models.

However, the oxygen-rich remnants have proven to be very difficult ultraviolet targets (cf. Blair and Panagia 1987). Some objects are hopelessly too faint or reddened to be detectable by *IUE* (Cas A: $A_v \sim 4.3$). Others, such as 0540−69.3 in the LMC, have been attempted without success although the reason for failure is not entirely clear: with no Balmer line emission, the reddening is not well known and could be the problem. The LMC remnant N132D was recently detected with *IUE* after an earlier unsuccessful attempt (Blair *et al.* 1988). The SNR in NGC 4449 was observed by Blair *et al.* (1984), but only the O III] λ1664 line was seen against the bright H II region background. Even so, the upper limits on other lines in the ultraviolet were used to constrain some characteristics of the precursor star.

For 1E 0102.2−7219, some direct information on the extinction is available. Tuohy and Dopita (1983) observed a faint halo of emission directly adjacent to the SNR and found Hα/Hβ = 2.9, which is nearly the recombination ratio. Hence, the reddening must be quite small. Also, the optical filaments have reasonably high surface brightness in [O III] λ5007, which led us to believe it should be detectable with *IUE*. In § II, we discuss our *IUE* and optical observations of 1E 0102.2−7219. Section III follows with a discussion and comparison with model calculations.

II. OBSERVATIONS AND DATA REDUCTION

a) Ultraviolet

The *IUE Observatory* has been described by Boggess *et al.* (1978), with much updated information available in the *IUE Newsletter* series. A log of the *IUE* exposures in and around 1E 0102.2−7219 is given in Table 2. The SNR was first observed during the seventh round of *IUE* on program NSGWB. The exposure for SWP 23925 was intended to be much longer, but the combination of a difficult blind offset maneuver and unexpected high background in the US1 shift limited the integration to just under 5 hr. The resulting spectrum was very noisy. Also, a faint star contaminated part of spectrum: this star was anticipated to be just outside the aperture, so a slight error in the blind offset maneuver or the astrometry is indicated. Even so, careful inspection of the photowrite image and the line-by-line file convinced us that some faint, extended emission due to the SNR was present at 1550 Å, 1909 Å, and possibly several other wavelengths. The smoothed, extracted spectrum for lines 30–34 (55 line format) of SWP 23925 is shown in Figure 1. While the quality of this spectrum is poor, the experience gained from the set-up and analysis of the resulting spectrum was crucial to the ultimate success of our eighth round program.

For the eighth round, we combined pairs of back to back ESA and US1 shifts to obtain long SWP and LWP exposures of the SNR. The observations were scheduled to permit the long dimension of the large aperture to be roughly aligned along the bright southeastern rim of the [O III] ring visible in Tuohy and Dopita's (1983) photograph, while also being mindful of the spacecraft β angle requirements. The position angle for the long dimension of the large aperture during each exposure (degrees east of north) is given in Table 2. During each of the long SNR exposures, long serendipitous exposures were obtained with the other camera at positions $\sim 1'.1$ away. The aperture orientations and relative positions are shown schematically in Figure 2.

In retrospect, the SNR slit position was not as ideal as it might have been—a position a few arcsec to the south and west would have incorporated more SNR emission in the large aperture. This slight misplacement is due to two factors: (1) We wanted to avoid the star that had contaminated our seventh round spectrum (believed to be the star on the southwest edge of the [O III] ring), and probably moved further east than absolutely necessary. (2) Dopita, Tuohy, and Mathewson (1981) give an astrometric position for the center of the [O III] ring measured from a fit to nearby SAO stars. (This adopted

TABLE 2

IUE EXPOSURE LOG FOR 1E 0102.2−7219 REGION

Image Number	Date	Exposure (minutes)	LGAP Position Angle	Comments
SWP 23925	1984 Sep 10	295	−137°	Seventh round trial exposure
SWP 27926	1986 Mar 16	865	52	SNR position
LWP 7803	1986 Mar 16	852	52	Serendipitous exposure NE of SNR
SWP 27971	1986 Mar 21	790	59	Serendipitous exposure SW of SNR (in N76A H II Region)
LWP 7845	1986 Mar 21	840	59	SNR position

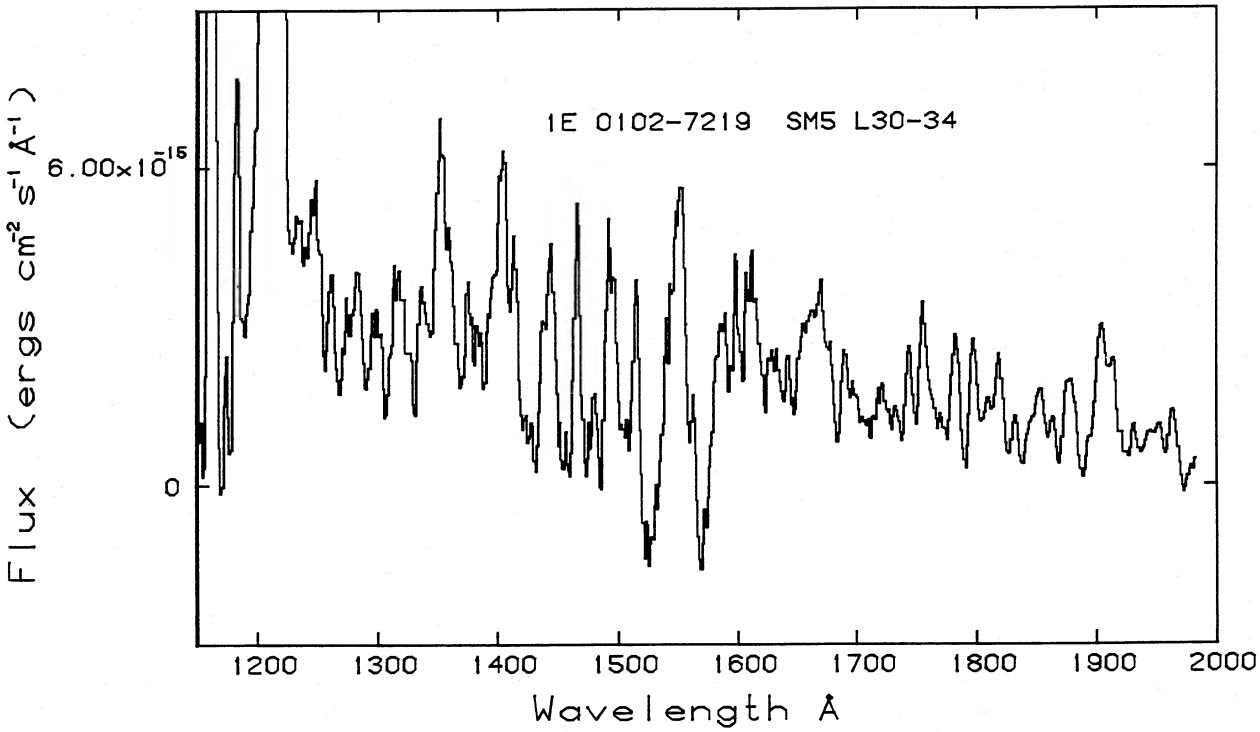

FIG. 1.—Extraction of lines 30–34 from SWP 23925, smoothed over 5 pixels. Although the spectrum is very noisy, all of the emission lines identified in our longer SWP exposure are also visible here.

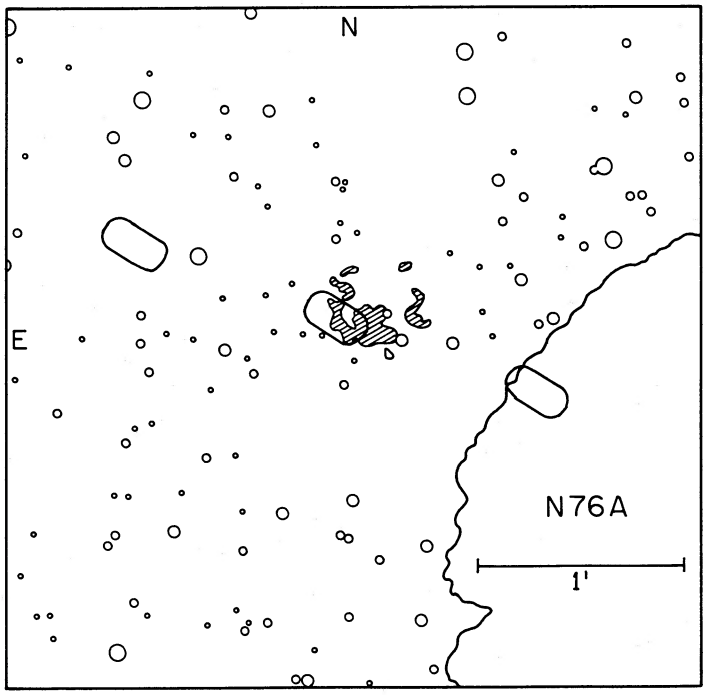

FIG. 2.—Schematic diagram of Tuohy and Dopita's (1983) [O III] photograph of the region surrounding 1E 0102−7219 (their Fig. 6), showing the aperture positions for the *IUE* exposures listed in Table 2. The cross-hatched regions denote emission due to the SNR. The aperture positions to the northeast and southwest show the locations of the serendipitous exposures.

center is shown in Mathewson *et al.* 1983.) Although Dopita, Tuohy, and Mathewson (1981) do not quote an accuracy, such fits are usually good to $\lesssim 2''$ rms. This was the best coordinate available at the time of our observation and the *IUE* slit position was measured relative to their assumed center. The resulting spectra only showed emission over part of the large aperture (see below). A subsequent evaluation of our pointing using our own astrometry (rms = 1".25) and information on the observing log has led to the aperture position shown in Figure 2. Our position for the ring center as indicated by Mathewson *et al.* (1983) is $\alpha = 01^h02^m25^s0$, $\delta = -72°18'04''.6$ (1950), different from Dopita *et al.*'s position by about 5". Our best estimate of the actual coordinate of the center of the *IUE* large aperture for the SNR exposures is $\alpha = 01^h02^m27^s3$, $\delta = -72°18'06''.8$ (1950), which is centered on the high surface brightness southeastern rim of the [O III] ring.

The positions for the serendipitous exposures were fixed by the aperture orientation and the known separation of the long-wavelength and short-wavelength camera's large apertures. LWP 7803 was obtained at a position northeast of the SNR, as shown in Figure 2. This is essentially a blank sky position, although the outermost portions of the "halo" discussed by Tuohy and Dopita (1983) are visible in this region. The spectrum shows no emission lines, but very faint, diffuse continuum can be seen for $\lambda \geq 2500$ Å. SWP 27971 was taken to the southwest of the SNR, in the outer portion of the bright SMC H II region N76A. This spectrum shows faint, diffuse continuum nearly filling the aperture over the entire SWP wavelength range, presumably due to dust scattered light from blue stars in the H II region. The only emission line present is C III] λ1909, which shows as a slight enhancement over the diffuse background.

Based on the experience gained from our seventh round exposure, the set-up for the SNR exposures was straightforward and integrations of ≥ 14 hr were obtained with both the SWP and LWP cameras. Because of the long exposures, the background levels are fairly high ($\sim$160 DN for SWP 27926 and $\sim$185 DN for LWP 7845), but emission lines from the SNR are clearly visible on the photowrites as diffuse patches of emission extending over roughly half of the spatial dimension of the large aperture. A faint, diffuse continuum is also apparent on the photowrites. Given that diffuse continuum was seen filling the large aperture in both serendipitous exposures, it is tempting to attribute this continuum to dust-scattered starlight. However, there are two differences between the continuum seen in the SNR exposures and that seen in the serendipitous exposures. First, the continuum in the SNR exposures shows a noticeable variation in spatial dimension of the large aperture, being brighter on the side closest to the small aperture. (Using information from the *IUE* Observer's Guide, this is the end of the aperture toward the southwest—see Fig. 2.) Second, the continuum emission does not appear to fill the large aperture, but only extends over the same portion of the aperture as the emission lines. This is especially clear in the LWP spectrum, for which the focus seems somewhat crisper. In this spectrum, the brightening of the continuum toward the small aperture side appears almost stellar. Comparison of the aperture position to the Hα image of Dopita, Tuohy, and Mathewson (1981) (which shows mainly stars) does not show a star at or near this position, but a better continuum image is necessary for clarification. Nonetheless, a diffuse continuum is clearly present, and we believe that at least this component is attributable to the SNR.

Most of the emission lines are visible in the standard IUESIPS reduction, but we have re-extracted the spectra from the line-by-line data file on the guest observer tapes in order to optimize the signal-to-noise ratio of the resulting spectra. These reductions were performed at the RDAF facility at NASA/GSFC. Using cross cuts in the spatial dimension at the positions of apparent emission lines, the extent of the SNR emission was measured and line numbers for the extraction chosen. With the change in *IUE* data format to 110 lines, the SWP and LWP large apertures are centered at line 55 and extend for ± 15 lines. In SWP 27926, SNR emission was identified in lines 51–65, while for LWP 7845 the emission lines extend from line 46 to line 60. In both cases, the emission extends over roughly half of the large aperture, and the relatively clean edges of the emission in the spatial direction are not due to the edge of the aperture.

The extracted short-wavelength spectrum is shown in Figure 3 after removal of hits and reseau marks and after smoothing over three pixels. The strongest line is C IV λ1550, and C III] λ1909 and the Si IV/O IV] features at λ1400 are also seen protruding from a noisy continuum. The most surprising feature in this spectrum is the strong line at $\sim$1354 Å which we identify as a recombination line of O I (see next section). Conspicuous by its weakness or near absence is the O III] λ1664 line, which was the only line detected in the ultraviolet spectrum of the SNR in NGC 4449 (Blair *et al.* 1984). The apparent weakness of this line is partly an artifact of the reduction process. The O III] line is nearly always affected by some "hot pixels" that are well documented and often are seen in long SWP exposures at 1664 Å. These hot pixels were removed manually from the line-by-line data before the spectrum was reextracted. However, because the continuum is very noisy in each individual line spectrum, it is very difficult to subtract these hot pixels accurately. Careful inspection of the photowrite image indicates that λ1664 is probably present at about the same intensity as λ1909, although this is not reflected in Figure 3. This is consistent with the spectrum shown in Figure 1 which was not as affected by hot pixel contamination.

The extracted long-wavelength spectrum of the SNR is shown in Figure 4. Again, hits and reseaux have been removed, and smoothing over 3 pixels has been applied. Three lines belonging to the SNR have been detected: [Ne IV] λ2420, Mg II λ2800, and [O II] λ2470. The spectrum is very noisy below $\sim$2400 Å, but there is no evidence of C II] λ2325. The faint continuum is also apparent in Figure 4.

The short-wavelength and long-wavelength spectra are shown merged together in Figure 5. Additional smoothing has been applied and the "features" in the 2100–2400 Å range arise from blended noise and are not believable. However, this figure demonstrates that a slight dip is present in the continuum over the 2000–2300 Å range; this corresponds to the position of the "2200 Å bump" seen in extinction curves and probably indicates a small amount of reddening is present. The source of the extinction could be Galactic, internal to the SMC, or a combination of both.

Tuohy and Dopita (1983) found Hα/H$\beta = 2.9$ and T_e(O III) $\geq$ 15,600 K for the halo adjacent to the SNR. Using data from Osterbrock (1974, Table 4.4), the intrinsic ratio for case B recombination would be 2.78, which implies a color excess of at least $E(B-V) = 0.04$). A number of stars in the SMC have been observed with *IUE* for purposes of studying extinction (Rocca-Volmerange *et al.* 1981; Nandy *et al.* 1982; Hutchings 1982; Prevot *et al.* 1984), and the smallest color

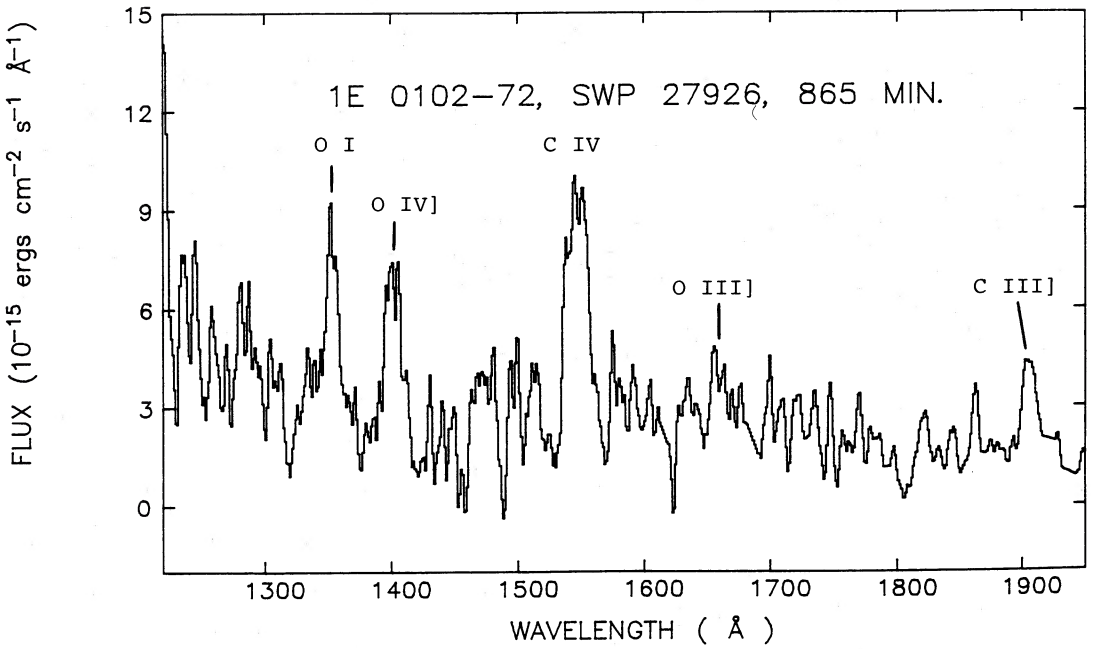

FIG. 3.—Extraction of lines 51–65 from SWP 27926, smoothed over 3 pixels. SNR emission lines are indicated. The O III λ1663 line may be underestimated (see text). Note the faint continuum emission.

excesses are 0.04–0.06; this is presumably due to our Galaxy. Four stars within 15′ of the SNR have been observed with *IUE*, and for these stars the mean color excess is $\langle E(B-V)\rangle_{UV} = 0.06$. The optical reddening estimates for these same stars are systematically higher, with $\langle E(B-V)\rangle_{OPT} = 0.14$. For the discussion that follows, we will adopt $E(B-V) = 0.08$ and assume that half of the reddening is from our Galaxy (Seaton 1979) and half is internal to the SMC (Prevot *et al.* 1984). This is a small amount of extinction, but the differential extinction between ultraviolet and optical is large enough that relative line intensities can be affected.

The observed integrated ultraviolet line intensities are shown in Table 3, scaled relative to $F(1909) = 100$. Because the continuum is so noisy and the integrated fluxes are sensitive to the placement of the continuum, the ultraviolet line intensities are accurate only to 30%–50%. Conservative upper limits for additional lines of interest are also given, as well as reddening corrected line intensities, $I(\lambda)$, scaled to $I(1909) = 100$.

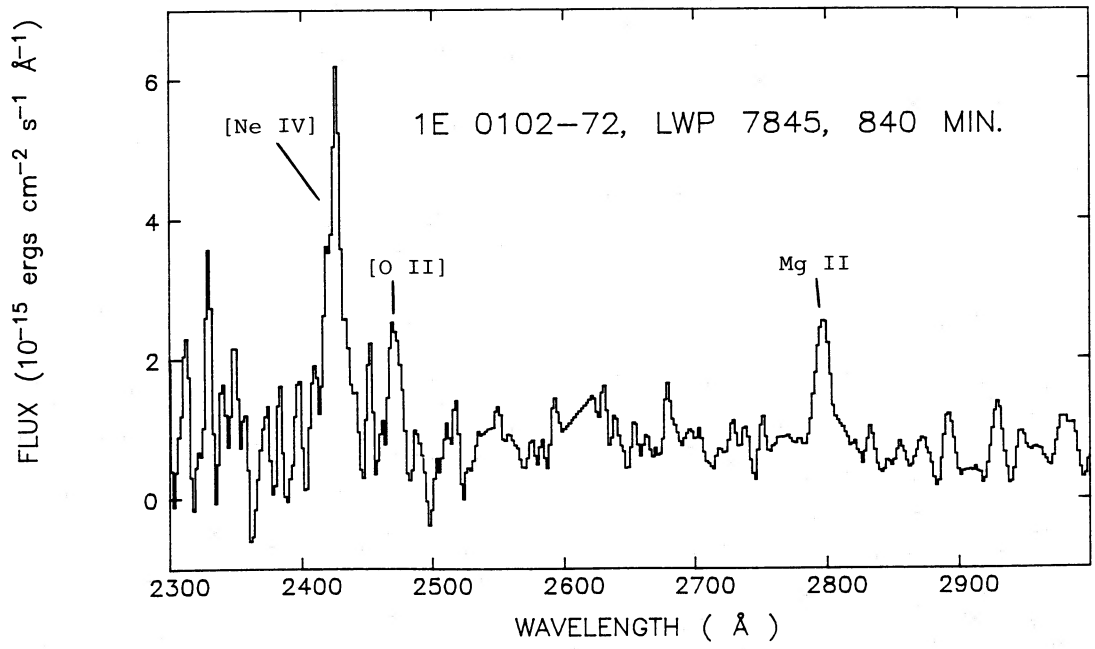

FIG. 4.—Extraction of lines 46–60 from LWP 7845, smoothed over 3 pixels. SNR emission lines are indicated. A bad "hit" has been removed just longward of 2600 Å.

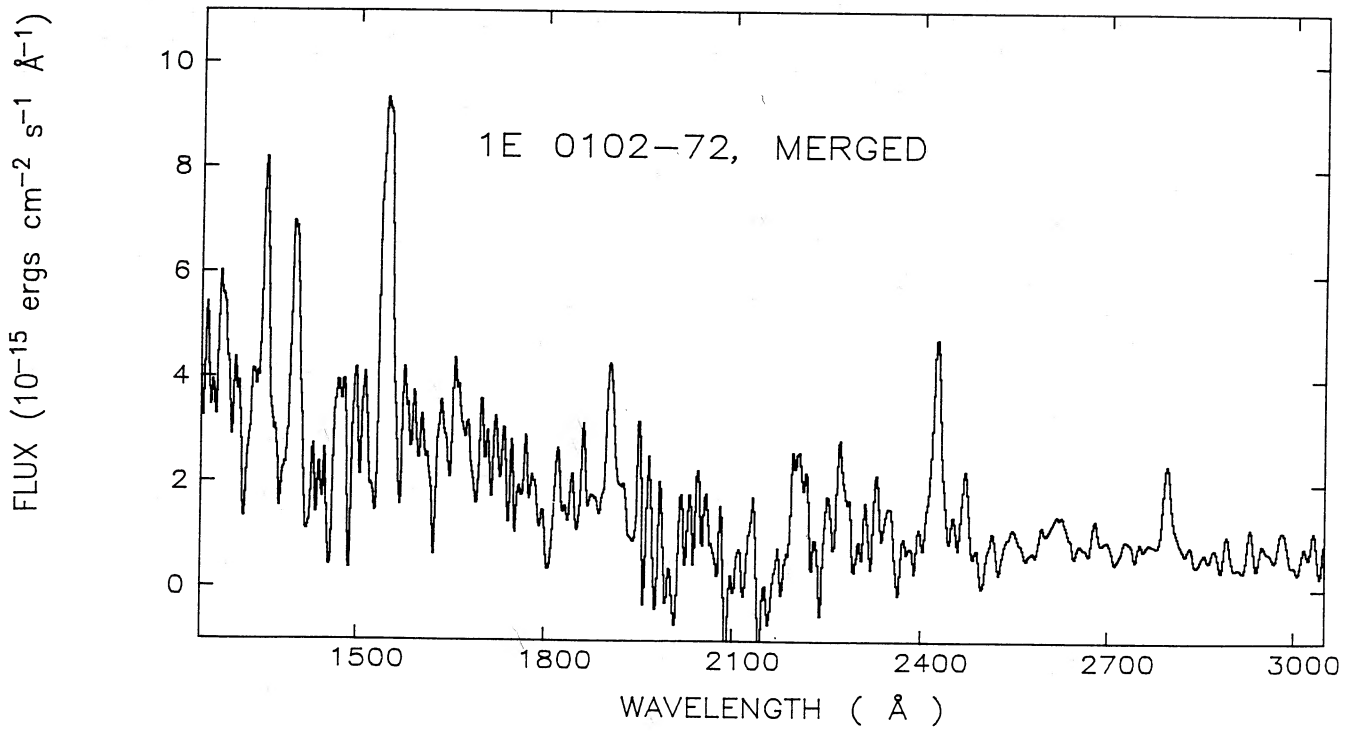

FIG. 5.—Overall UV spectrum of 1E 0102−7219, after additional smoothing. The features in the 2200–2300 Å range are apparently due to noise blended in the smoothing process and are not real.

b) *Optical*

A long-slit spectrum of the object was obtained in 1984 November using a CCD spectrograph on the CTIO 4 m telescope. The slit width of 300 μm (corresponding to $\sim$2″) and the 158 line mm^{-1} grating produced a spectrum of the 6700–10000 Å region with about 5 Å resolution. The integration time was 2700 s. The long east-west slit cut through the south central part of the optical emission, essentially passing just south of the center of the *IUE* LGAP position shown in Figure 2.

These data have been reduced using IRAF on a microVax at the Center for Astrophysics. The data were flat-fielded and bias-subtracted following standard procedures, and calibrated using spectra of Stone and Baldwin (1983) standard stars observed the same night. Standard extinction values for CTIO were assumed.

Although the object is faint and the sky contamination gets worse as one goes into the red, these long slit data permit good sky subtraction. We have extracted the region of the long slit corresponding to the SE portion of the remnant (roughly where the long slit intersects the *IUE* aperture), and show this spectrum in Figure 6. The sky subtraction is reasonably good out to $\sim$9200 Å. In addition to the [O II] λ7325 blend, the O I *recombination* line at 7774 Å is clearly seen and a corresponding O I line at 8446 Å is also present. No other features are clearly seen above the level of the noise, although another O I line at 9262 Å may be present.

The presence of permitted O I lines is quite interesting. The O I λ8446 line has been seen in some novae and AGNs and is attributed to Lyβ pumping of this transition (Strittmatter *et al.* 1977; Grandi 1980). However, the only SNR known to show permitted O I is Puppis A: Winkler and Kirshner (1985) detected the lines in their spectra of an oxygen-rich knot, with a ratio of $\lambda7774/\lambda8446 \approx 2$. This cannot be due to Lyβ pumping, and since the ratio is consistent with the statistical weights of these lines (=5/3), optically thick recombination was implicated.

In our case, the ratio of the O I lines is even more extreme, with $\lambda7774/\lambda8446 \geq 3.5$. This can be understood if the recombining gas is at least partially optically thin to O I resonance lines. Julienne, Davis, and Oran (1974) have calculated effective

TABLE 3

UV LINE INTENSITIES FOR 1E 0102.2−7219

Ion	Laboratory Wavelength	Measured Centroid	Measured Width	$F(\lambda)$	$I(\lambda)$
N V	1240	...	...	<30	<42
Si III	1262	...	...	<30	<41
O I	1304	...	...	<30	<39
C II	1335	...	...	<30	<38
O I	1356	1352.7	4.0	153	191
Si IV/O IV]	1398/1403	1402.1	5.8	247	297
N IV]	1486	...	...	<50	<57
C IV	1549	1547.3	7.0	449	490
He II	1640	...	...	<20	<21
O III]	1664	1661.0	4.0	75	79
N III]	1748	...	...	<20	<20
Si III]	1892	...	...	<10	<10
C III]	1909	1905.9	4.3	100	100
C II]	2326	...	...	<50	<47
[Ne IV]	2425	2426.2	5.6	191	172
[O II]	2470	2471.6	3.7	62	55
Mg II	2798	2797.9	6.1	74	60
C I]	2966	...	...	<20	<16

NOTE.—$F(1909) = 3.4$ E−14 ergs cm^{-2} s^{-1}; $I(1909) = 5.9$ E−14 ergs cm^{-2} s^{-1}. Reddening correction assumes $E(B-V) = 0.04$ (Galactic) + $E(B-V) = 0.04$ (SMC); see text.

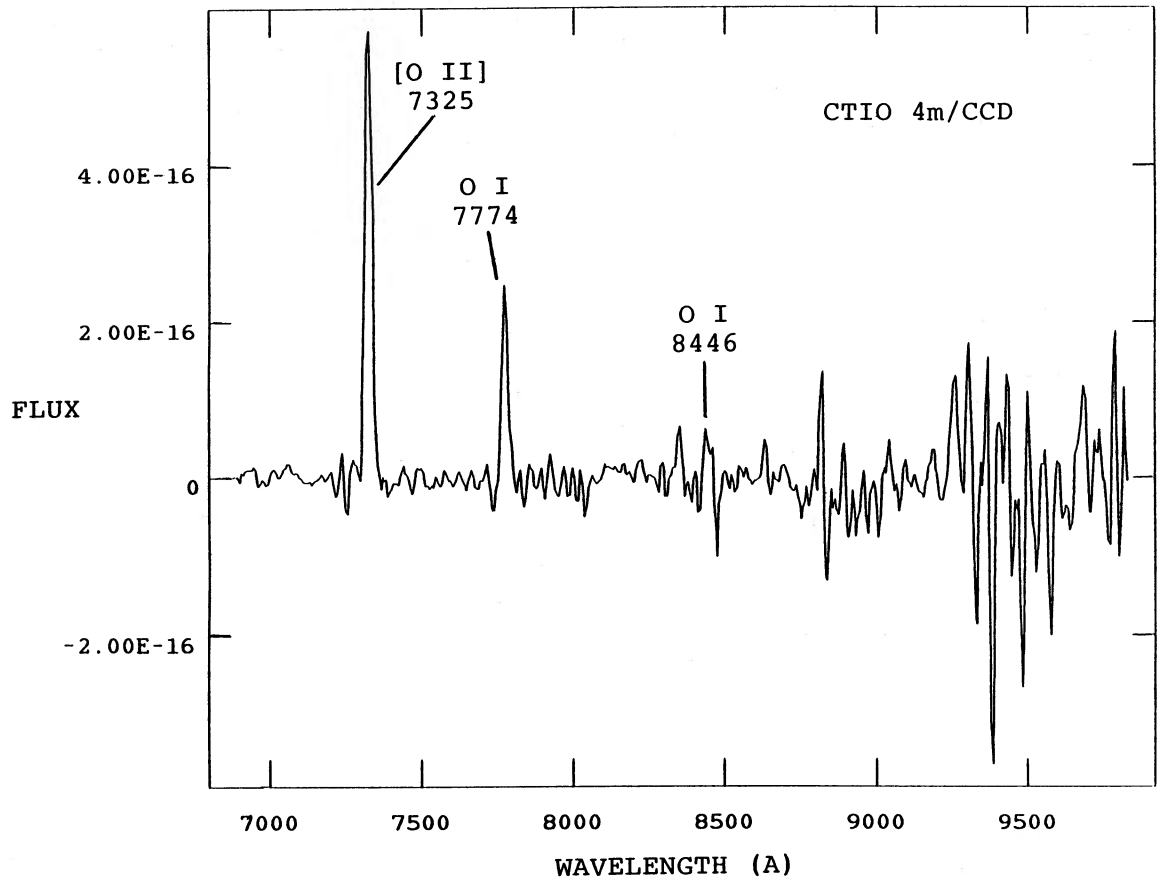

FIG. 6.—Optical/near-IR spectrum of 1E 0102−7219 obtained with a long-slit CCD spectrograph on the CTIO 4 m telescope. Note the O I recombination lines.

recombination coefficients for these lines for a temperature of 1160 K both optically thick and optically thin situations. Winkler and Kirshner (1985) scale these coefficients to 10^4 K using a $T^{-0.9}$ law (Gould 1978; note however that Gould uses $T^{-0.5}$), choosing 10^4 K because of the observed ratio of [O II] λ7325/O I λ7774 = 7.2. In our case, this ratio is much lower (2.8), implying a lower temperature. Hence, we will use the coefficients of Julienne, Davis, and Oran (1974) directly. For the optically thick case, the ratio of recombination coefficients is $\alpha(7774)/\alpha(8446) = 1.85$, consistent with Winkler and Kirshner's (1985) observation in Puppis A. For the optically thin case, this ratio is 10.7. The observed ratio for 1E 0102−7219 thus implies partially thin conditions.

c) *Optical to Ultraviolet Scaling*

Interestingly, partially thin O I recombination provides a natural explanation for an apparent peculiarity of the ultraviolet spectrum, and also permits a reasonable relative scaling of the ultraviolet and optical line intensities. The most reasonable identification for the strong line at 1354 Å in the IUE spectrum is the O I recombination line at 1356 Å. However, in many situations where O I recombination is seen, the O I λ1304 line is seen to be stronger than λ1356, and no λ1304 line is detected in our spectrum. (Note that this contrasts sharply with a spectrum of N132D we recently obtained, in which the λ1356 line could not be detected.) In the recombination cascade, the λ7774 line feeds λ1356 while λ8446 feeds λ1304 (cf. Julienne and Davis 1976). Since the λ8446/λ7774 ratio decreases for the optically thin case, so does the λ1304/λ1356 ratio. Using the recombination coefficients of Julienne, Davis, and Oran (1974) again, the optically thick case gives $\alpha(1356)/\alpha(1304) = 1.75$, implying that λ1304 should have been detected in our spectrum. However, in the optically thin case, the ratio of coefficients is 10, which can more than account for the absence of λ1304.

Since λ7774 is the main line feeding λ1356, the relative intensities of these lines can be used to scale the optical and ultraviolet line intensities. The differences between the aperture sizes and orientations cause some concern in this procedure, since variations in relative line intensities may occur from one position to another. However, the ultraviolet spectrum covers a substantial portion of the SE region of the SNR and both our own optical data and that presented by Dopita and Tuohy (1984) indicate that the optical line variations are present but not extreme on observable spatial scales ($\sim$2″). We thus have confidence that this procedure should produce a reasonable comparison of global line intensities.

The ultraviolet to optical scaling has been accomplished assuming a theoretical ratio of

$$\frac{I(1356)}{I(7774)} = \frac{\alpha_{\rm rec}(1356)}{\alpha_{\rm rec}(7774)} \times \frac{E_{\rm ph}(1356)}{E_{\rm ph}(7774)} = 5.9\,, \qquad (1)$$

where $\alpha_{\rm rec}$ are the effective recombination rate coefficients from Julienne, Davis, and Oran (1974) and $E_{\rm ph}$ is the energy per photon. Since both transitions are quintets, they are unaffected by the degree to which the gas is optically thin. (Note that the other quintet line at 9264 Å may also be present in Fig. 6

TABLE 4

RELATIVE UV TO OPTICAL LINE INTENSITIES FOR 1E 0102.2−7219

Ion	λ	$F(\lambda5007 = 100)$	$I(\lambda5007 = 100)$
N v	1240	<2.4	<4.4
Si III	1262	<2.4	<4.3
O I	1304	<2.4	<4.2
C II	1335	<2.4	<4.0
O I	1356	12.1	20.2
Si IV/O IV]	1400	19.6	31.5
N IV]	1486	<4.0	<6.0
C IV	1549	35.7	52.0
He II	1640	<1.6	<2.2
O III]	1664	6.0	8.4
N III]	1748	<1.6	<2.2
Si III]	1892	<0.8	<1.1
C III]	1909	8.0	10.6
C II]	2326	<4.0	<5.0
[Ne IV]	2425	15.2	18.3
[O II]	2470	4.9	5.8
Mg II	2798	5.9	6.4
C I]	2966	<1.6	<1.7
[Ne III], [Ne V]	3345	6.3	7.2
[Ne V]	3426	9.5	10.8
[O II]	3727	150	164
[Ne III]	3869	19.0	20.7
[Ne III]	3968	5.5	5.9
[O III]	4363	4.6	4.8
Mg I	4571	1.0:	1.0:
[Ne IV]	4725	1.4:	1.4:
[O III]	4959	32.2	32.3
[O III]	5007	100	100
[O I]	6300	5.0	4.7
[O I]	6363	1.6:	1.5:
[O II]	7320, 30	10.0	9.0
O I	7774	3.6	3.2
O I	8446	≤0.9	≤0.8
O I	9246	≤2.2	≤2.0
[S III]	9532	≤2.3	<2.0

NOTES.—(1) A colon (:) denotes especially uncertain values. (2) UV to optical scaling assumes a theoretical ratio of $I(1356)/I(7774) = 5.9$. (3) Reddening correction assumes $E(B-V) = 0.04$ (galactic) plus $E(B-V) = 0.04$ (SMC).

although the noise in this part of the spectrum makes it difficult to say for certain.) This theoretical ratio was reddened assuming extinction as discussed in § II*a* above. The observed line strengths were then scaled to this reddened value, and the other optical data was tied to this using relative intensities of lines in overlapping regions of spectra. Using Dopita and Tuohy's (1984) global spectrum of 1E 0102−7219 (especially below 3700 Å) in conjunction with our optical and ultraviolet data yields the total line list presented in Table 4, scaled relative to $I(5007) = 100$. These line intensities form the basis for the discussion that follows.

III. ANALYSIS AND MODELS

There are two apparent sources for the energy which the supernova ejecta is radiating—shock heating or photoionization. Neither is entirely satisfactory to explain the observed line intensities, so a combination may be needed, but we consider each in turn.

a) Shock Waves

Shocks are a natural explanation for the observed emission in that the ejecta encounter a "reverse" shock when they overtake the decelerating high pressure shell of swept-up interstellar material (McKee 1974; Gull 1975). While most of the material passing through the reverse shock becomes so hot it emits at X-ray, rather than optical, wavelengths, the slower shocks in dense clumps of ejected gas can produce optical emission. Chevalier and Kirshner (1978) interpreted the fast-moving knots in Cas A as such shocks, and this picture is supported by the sudden appearance and disappearance of many of these knots (van den Bergh and Kamper 1983).

Itoh (1981) has constructed models of radiative shock waves in pure oxygen and extended them to include the O I λ7774 recombination line (Itoh 1986). Dopita, Binette, and Tuohy (1984, hereafter DBT) computed models for the mixture of carbon, oxygen, and oxygen-burning products expected for a 25 $M_\odot$ precursor. A major uncertainty in the models is electron-ion equilibration. One can assume (1) instant equilibration of electron and ion temperatures throughout the shocked gas, (2) energy exchange between electrons and ions by Coulomb collisions alone, or (3) complete equilibration in the shock front itself, but only Coulomb equilibration in the cooling zone. The pure Coulomb models are especially remarkable in having an extensive region of nearly constant electron temperature, with heating by collisions with ions balancing radiative cooling. We have used a modified version of the radiative shock code described in Cox and Raymond (1985) to compute a few models with higher or lower shock velocity than those of Itoh or DBT, models with different abundance sets, and models which include the observed X-ray emission of 1E 0102.2−7219. The X-ray radiation leads to strong Auger ionization. (The X-ray spectrum assumed is discussed in the next section.) All these models assumed instant electron-ion equilibration. Aside from confirming the published models, we find that the X-ray emission alone can completely ionize any gas less dense than about 1.0 cm^{-3}, so that even precursors of very slow shocks can be ionized.

One model of the DBT set, the 42.5 km s^{-1} complete equilibration model S2B, provides a reasonable match to the observed optical lines. The [O II] λ3727 doublet is 3 times the [O III] λ5007 strength (somewhat stronger than observed, while [O I] λ6300 is a few percent as strong as [O III]. The temperature sensitive [O II] and [O III] line ratios also agree quite well with those observed. We ran a similar model which included X-ray ionization and assumed a preshock density of 10 cm^{-3}, rather than 0.1 cm^{-3} used by DBT. This model gave a far less satisfactory fit, probably because the preshock gas was more highly ionized, and the [O II] and [O I] intensities relative to [O III] were reduced by one and two orders of magnitude, respectively. For the same reason, the O I λ7774 recombination line in our model was far too weak, but an arbitrarily large amount of cold, compressed, nearly neutral gas could trail the shock, and X-ray ionization of this gas could provide the necessary recombinations.

Further problems arise in attempting to match the observed high ionization species Ne IV and Ne V, and in matching the ratios of ultraviolet lines to the optical. Models which produce [O II]/[O III] and [O I]/[O III] comparable to the observed values predict no emission at all in [Ne IV] or [Ne V], because the gas never reaches high ionization states. Models which collisionally ionize oxygen to O^{++} have high enough temperatures to excite strong UV emission, but the observed UV lines are rather weak. The cleanest example is the O III] λ1664/[O III] λ5007 ratio. While the shock models typically predict a value of 0.6, the observed value is 0.08. The [Ne IV] and [Ne V] problem could be explained by assuming a wide range of shock velocities within the observed volume, as in the curved shocks of Herbig-Haro objects (Hartigan, Raymond, and

Hartmann 1987). However, any shocks which produce these lines would give a C IV λ1550/C III] λ1909 ratio far larger than observed, and a mixture of different shock velocities would not alleviate the problem with the O III λ1664/λ5007 line ratio.

A model in which gas photoionized by X-rays is heated by very slow shocks to temperatures of 20,000–30,000 K might work, but then one has to consider whether the shock is necessary at all. Therefore, we turn now to photoionization models.

b) *X-Ray Photoionized Gas*

The 1.5×10^{37} ergs s^{-1} X-ray luminosity of 1E 0102.2−7219 (Hughes 1987) implies an X-ray flux of order 0.02 ergs cm^{-2} s^{-1} within the [O III] emitting ring (assuming a ring geometry with a height about 10% the radius). The ratio of X-ray flux to density is far higher in 1E 0102.2−7219 than in other known oxygen-rich SNRs, and photoionization is correspondingly more important. Detailed measurements of the X-ray spectrum are not available, so we have used the X-ray emission code of Raymond and Smith (1977), with updated atomic data summarized by Cox and Raymond (1985) to generate model spectra covering the 5–1000 eV energy range at 2.1 eV resolution. The X-ray–emitting gas is likely to be far from ionization equilibrium (e.g., Itoh 1977; Gronenschild and Mewe 1982), since the observed X-ray luminosity requires a density of only ~ 1 atom cm^{-3}. Models of young SNRs generally show very strong emission from the helium-like ions of the elements present (e.g., Hamilton, Sarazin, and Chevalier 1983; Hughes and Helfand 1985), so we have added the emission of carbon in a 10^6 K plasma, oxygen at 1.6×10^6 K, and neon at 3×10^6 K to give a spectrum resembling those predicted by models. The adopted flux was 0.01 ergs cm^{-2} s^{-1} in the O VII and O VIII lines, 0.013 ergs cm^{-2} s^{-1} in the Ne IX and Ne X lines, and 0.008 ergs cm^{-2} s^{-1} in the two-photon, recombination, and bremsstrahlung continua of these elements. The emission in the C V and C VI lines is not included in the measured fluxes because both the *Einstein* IPC and HRI are insensitive just above the carbon edge. Lacking any good constraint on the carbon line flux, we scaled the carbon line flux to 0.007 ergs cm^{-2} s^{-1}, so that it is comparable to the fluxes of the observed lines, but not dominant. Several variants on this X-ray spectrum were used to examine the sensitivity of the results to the assumed X-ray spectrum. In particular, we tried much stronger carbon line emission, strong EUV emission in lines such as O V λ630, and attenuated EUV emission to simulate the effects of absorption by the optically bright gas. These alternatives changed the equilibrium temperatures of the photoionized gas by $\lesssim 30\%$ and some of the line ratios by factors of 2, but they do not alter the general conclusions below.

The X-ray spectrum was used to compute the equilibrium ionization state and heating rate of gas at various densities, and the temperature was iterated until radiative cooling balanced the heating. The abundances assumed by number were (following DBT) C:O:Ne:Mg:Si:S = 0.2:1.0:0.63:0.08:0.025:0.0063. K shell photoionization followed by Auger ionization dominates the heating because of the large photon energy involved. Most of the atomic processes included are summarized in Cox and Raymond (1985). Of particular importance here are K shell photoionization leading to Auger ionization (Daltabuit and Cox 1972; Reilman and Manson 1979), low-temperature dielectronic recombination (Nussbaumer and Storey 1983, 1984), and cooling by electron impact excitation. The recombination contributions to the line emissivities must also be included. At very low temperatures free electrons tend to recombine into excited levels and cascade down. Therefore, with the exception of the O I lines discussed above, we split up the total recombination rate among the accessible levels by statistical weight. For example, recombination to O III is assumed to go $\frac{3}{4}$ to the triplet states and $\frac{1}{4}$ to the singlets, while the quintuplets cannot be reached by adding one electron to the ^2P ground level of O IV. It should be noted that the O III] λ1664 and O IV] λ1400 lines cannot be formed by recombination, and their presence provides direct evidence that recombination in cold, ionized gas does not account for all the emission, as it does in some nova shells (Ferland *et al.* 1984).

We also include the charge transfer process

$$O + O^{++} \rightarrow 2O^{+}$$

at the rate given by Fox and Victor (1981). Other charge transfer reactions not usually important in astrophysical plasmas could be significant in the carbon-oxygen-neon plasma, but the rates are not known.

Some typical results are shown in Table 5. The gas in the remnant probably spans a wide range in density. Regions denser than about 10 cm^{-3} produce the O I recombination lines, but they are too cold to produce any line excitation except in the far-infrared. Regions near 1 cm^{-3} are warm enough to produce the observed ultraviolet lines, but the temperatures are low enough that the UV-to-optical line ratios are modest. Gas spanning a wide density range can qualitatively account for the observed spectrum. A fraction on the order of 10% of the apparent volume of a torus 3.5 pc in radius with a minor radius one-tenth as large containing gas at a density $n_0 \sim 1$ cm^{-3} can account for the observed [O III] optical

TABLE 5

PHOTOIONIZATION EQUILIBRIUM SUPERNOVA EJECTA EMISSIVITY[a]

		MODEL				
		A	B	C	D	E
		$n_e = 59.$	19.	5.1	3.5	2.2
		$n_0 = 30.$	6.0	1.0	0.6	0.3
		$T = 1590$	6250	12400	15600	22000
		$n_e n_0 = 2.7$	44000	5500	3000	1400
ION	λ	$n_e n_0 = 2.7 \times 10^5$				
C II	1335	...	0.30	19.	24.	18.
O I	1356	870.	19	0.5	...	...
Si IV	1400	27.	11	2.0	1.3	0.27
O IV]	1400	...	0.02	12.	31.	46.
C IV	1550	8.7	6.9	110.	180.	160.
O III]	1664	...	0.60	27.	34.	22.
Si III]	1890	54.	7.4	4.6	1.7	0.22
C III]	1909	140.	34.	90.	100.	67.
C II]	2325	...	6.9	120.	68.	24.
[Ne IV] ...	2425	2.6	8.1	110.	150.	120.
Mg II	2800	200.	120.	...	...	...
[Ne V]	3426	...	3.0	53.	89.	99.
[O II]	3727	120.	3000.	330.	120.	19.
[Ne III] ...	3969	18.	970.	470.	250.	66.
[O III]	4363	1.6	50.3	19.	16.	6.6
[Ne IV] ...	4725	0.8	1.1	1.4	1.6	1.2
[O III]	5007	8.5	3900.	1900.	660.	220.
[O I]	6300	130.	13.	2.1	0.12	...
[S II]	6723	1.6	2.0	0.03	...	...
[O III]	7325	22.	26.	8.6	4.2	0.86
O I	7774	170.	3.9	0.1	...	...
[S III]	9532	...	69.	0.30	0.03	...

[a] Emissivity in units of 10^{-23} ergs cm^{-3} s^{-1}.

luminosity, and similar volumes at higher densities can produce the oxygen recombination radiation and the UV lines.

It is not clear whether the full range of densities is present, or whether, by analogy with other X-ray ionized astrophysical plasmas, a thermal instability might occur (e.g., Krolik and Kallman 1984). The gas is expanding supersonically, so no large-scale thermal instability can occur, but on scales smaller than 10^{16} cm the gas might separate into cold and warm phases. Such a separation might stop, or at least slow down, as the gas becomes ionized. The resonance line of helium-like oxygen can K shell ionize the first three oxygen ions, but it lies just below the K shell threshold of O IV. Carbon and neon behave in a similar manner. Therefore, when the gas becomes more than twice ionized, the heating rate is significantly reduced if the X-ray spectrum is indeed dominated by emission from helium-like ions.

There are two major difficulties with the equilibrium photoionization models. First, the [O II] λ3727/[O III] λ5007 ratio is predicted to be less than about 0.3, while the observed ratio varies between 1.3 and 2. This reflects the fact that oxygen is mostly doubly ionized in models warm enough to effectively excite the λ3727 transition. Second, the [O III] emission comes mostly from 10,000–15,000 K gas in the model, but the I(4363)/I(5007) ratio suggests a temperature of 25,000 K. A recombination contribution to the λ4363 intensity helps to explain this discrepancy, but the amount predicted by the models is inadequate.

Both difficulties may be related to an unwarranted assumption of ionization equilibrium. While the heating and cooling time scales are a few years, so that thermal balance is a valid approximation, the ionization time scales are $\sim$2000 yr, which is close to the expansion age of the remnant. The difference in time scale arises because a single K shell photoionization deposits 1000 times the typical thermal energy of the particles in the plasma. Hence, time-dependent models should give a lower ionization state than predicted by the equilibrium model and also be somewhat warmer, since the thermal energy is shared among fewer particles.

We have run a series of time-dependent photoionization models using the atomic rates described above. Gas having the DBT abundances was allowed to expand freely at 3900 km s^{-1} for 2400 yr while exposed to the X-ray flux described above. The gas was initially taken to be cold and neutral. The initial conditions turned out to be irrelevant, however, since the gas always cooled quickly to the minimum temperature allowed by the code (630 K to avoid overflows in evaluating atomic rates), then slowly warmed and ionized late in the evolution.

Some model results are shown in Table 6. Again, a mixture of densities is needed to produce both the high ionization lines and the O I recombination lines. These particular models improve the [O II]/[O III] ratio, but still fall short of the observed value. They also predict a larger C III]/C IV ratio than observed and far too much C II] λ2325. These problems could be alleviated by increasing the carbon line intensities and decreasing the oxygen lines in the ionizing X-ray spectrum. However, considering the large number of free parameters, the possibility that the gas is optically thick at some wavelengths, and the likelihood that the X-ray flux changed with time during the evolution, we are loath to adjust the model parameters to try to "fit" the observed spectrum. A global model similar to Hamilton and Fesen's (1988) model for the absorption lines of SN 1006 would be more appropriate. However, the uncertain age, composition and geometrical structure of 1E 0102−7219 provide a large number of free parameters.

In summary, time-dependent photoionization by the EUV and X-ray radiation from the SNR can qualitatively explain the UV and optical line emission, but the density and ionization structures are complex and prevent a unique model from being specified. Many model parameters are poorly constrained, including the time dependence and shape of the ionizing spectrum. The incorrect prediction of such ratios as [O II]/[O III] and C II]/C III] can be attributed to incorrect parameter choices, missing atomic physics (e.g., novel charge transfer processes), or a significant role by shock waves in compressing and heating the gas. Moreover, the models presented here are not self-consistent in that the volumes and densities of the optically emitting gas imply optical depths of order unity in the EUV, but absorption of the ionizing radiation was ignored.

However, it is at least as likely that the shortcomings of the models in matching observations reflect a more fundamental limitation of the model assumptions. We have assumed throughout that the electron velocity distribution is Maxwellian and that the energy deposited by photoionization heats the electrons directly. In fact, the $\sim$500 eV electrons produced by the Auger process may excite or ionize other ions before they slow down enough to share their energy with other electrons. Based on the excitation and ionization cross sections of the first four ionization stages of oxygen, and on the Coulomb collision time scales (Spitzer 1978), we expect that most of the energy of the Auger electrons, especially in the low-ionization zones, would go into excitation and ionization rather than thermal heating. Many of the excitations would produce photons that could ionize lower ionization stages.

Monte Carlo calculations similar to those that have been performed for fast electrons in hydrogen and helium (Shull and

TABLE 6

PHOTOIONIZED SUPERNOVA EJECTA EMISSIVITY: TIME-DEPENDENT IONIZATION[a]

		Model				
		AA	BB	CC	DD	EE
		n_e = 22.	9.4	4.2	1.8	0.66
		n_0 = 9.4	3.1	0.94	0.31	0.094
Ion	λ	T = 630.	755.	8940.	15100.	23900.
C II	1335	...	...	1.6	2.0	21.
O I	1356	14.	10.	1.3	0.35	...
Si IV	1400	0.04	0.04	0.02	0.23	0.29
O IV]	1400	...	...	0.26	4.7	5.1
C IV	1550	0.13	0.14	0.36	5.6	7.5
O III]	1664	...	...	1.7	7.8	3.4
Si III]	1890	0.11	0.05	2.7	9.5	5.0
C III]	1909	1.00	0.52	4.4	22.	16.
C II]	2325	...	...	40.	64.	21.
[Ne IV]	2425	1.9	2.2	9.2	27.	11.
Mg II	2800	42.	6.7	8.8	0.12	...
[Ne V]	3426	0.26	0.34	5.5	15.	6.2
[O II]	3727	77.	26.	250.	59.	5.8
[Ne III]	3969	5.5	2.7	140.	68.	9.8
[O III]	4363	0.81	0.62	2.5	3.8	0.95
[Ne IV]	4725	0.58	0.68	0.02	0.26	0.21
[O III]	5007	4.3	3.3	500.	170.	20.
[O I]	6300	2.6	2.6	2.2	0.30	...
[S II]	6723	0.16	0.04	14.	2.9	0.35
[O II]	7325	14.	4.7	3.4	1.9	0.29
O I	7774	2.8	2.1	0.25	0.07	...
[S III]	9532	...	...	9.2	2.7	2.4

[a] Emissivity in units of 10^{-23} ergs cm^{-3} s^{-1}.

Van Steenberg 1985) are in progress (G. S. Victor and J. C. Raymond 1989, in preparation). Preliminary estimates based on calculations by G. Victor indicate the following: (1) The ionization rate in nearly neutral gas is much larger. In 1% ionized gas, ~50% of the energy goes into ionizing O I. The effect of this should be to make time-dependent ionization much less of a problem. (2) The observed [O II]/[O III] ratio should be much easier to obtain with the models that incorporate ionization. (3) A much lower mass of cold, neutral gas will be needed to make the O I recombination.

c) *Abundances*

In spite of the difficulties in arriving at a unique model for the optical and UV emission, we can derive some abundance estimates which are not seriously model dependent by choosing line ratios which are not too sensitive to temperature. We will use the equilibrium photoionization models, as they predict C II:C III:C IV and Ne III:Ne IV:Ne V ratios closer to the observations than do the shock wave or time-dependent photoionization models. The abundance estimates are summarized in Table 7.

The observed relative strengths of the neon lines agree reasonably well with the model, though the [Ne V] line is somewhat stronger than expected. Comparison of the [Ne III]/[O III] ratio with the models shows that a neon abundance slightly below that adopted would give a better fit. Therefore, we estimate Ne:O = 0.5.

The C III] and C IV lines are predicted to be 2.5–3 times stronger relative to the O III] and O IV] lines than observed, so the carbon abundance is lower than the DBT value assumed, and we will adopt C:O = 0.12.

The only other element detected is magnesium. Both the Mg I] and Mg II lines can be formed very effectively by recombination, or they can be collisionally excited at modest temperatures. Conveniently, the ratio of Mg II λ2800 to [O I] λ6300 is about the same in either case (models A and B), and we find that Mg:O = 0.1 (1.25 times the value assumed in the models) will match the observations.

Trace amounts of the elements not observed were included in the model calculations, and the predicted fluxes can be scaled to the observed upper limits. An upper limit to the hydrogen abundance is gotten from the failure to detect Hα. From the ratio of Hα to O I λ7774 predicted by model A, $0.8n_H/n_O$, we find H:O < 0.6 for case B hydrogen recombination. Similarly, the observation that $I(1640)/I(1356) < 0.1$ can be compared with the model A prediction $(0.09n_{He}/n_O)$ to give an upper limit He:O < 1, again for case B recombination. If the recombination in hydrogen and helium is optically thin in the Lyman lines due to large velocity gradients, the case A recombination coefficients would give upper limits one-third larger.

TABLE 7

DERIVED ABUNDANCES RELATIVE TO OXYGEN (BY NUMBER)

Element	Abundance
H	<0.6
He	<1
C	0.12
N	<0.01
O	1.0
Ne	0.5
Mg	0.1
Si	<0.03
S	<0.006
Ar	<0.017
Fe	<0.15:

The strongest upper limit to the nitrogen abundance comes from the lack of [N II] λ6584 emission. Assuming that Model B dominates the [O II] and [N II] emission, N:O < 0.001. However, the temperature indicated by the $I(7325)/I(3727)$ ratio is substantially higher, and N:O < 0.01 is a more realistic upper limit.

The ratio of Si III] λ1892 to C III] λ1909 is observed to be less than 0.1, while the models give $0.4n_{Si}/n_C$. Thus Si:C < 0.25 and Si:O < 0.03.

The [O III] emission is dominated by models B and C, and these should dominate the [Ar III] λ7136 emission as well. From the upper limit of 0.01 observed and the predicted value $0.6n_{Ar}/n_O$, we derive Ar:O < 0.017.

The strongest upper limit on the sulfur abundance comes from the failure to detect the [S III] line at 9532 Å. Assuming that about half the [O III] intensity arises in gas near the condition of model B, an observed upper limit for $I(9532)/I(5007) < 0.02$ translates into an upper limit S:O < 0.006.

It is also interesting to consider the emission of iron. In the photoionization models, it is not possible to hide arbitrary amounts of iron by assuming that they have not reached the reverse shock yet. The ionization state of iron is less well determined than those of the other elements, but comparison of the predicted [Fe III] lines with [O III] λ5007 suggests Fe:O < 0.15, but we consider this estimate highly uncertain.

d) *Mass*

The photoionization models also provide an estimate of the density at which a particular line is emitted, and therefore the amount of gas involved. The density derived depends on the X-ray flux assumed, and this is uncertain by a factor of 2 in either direction, but at least it provides a reasonable estimate. The [O III] emission is dominated by models B and C [though as mentioned above, the $I(4363)/I(5007)$ ratio suggests a higher temperature]. The [O III] λ5007 luminosity of 3×10^{35} ergs s^{-1} requires a volume of 8×10^{54} cm^3 at these temperatures. If we assume the [O III] radiation to arise in a ring 6.9 pc in diameter with height and thickness about one-tenth the radius, the [O III] emission comes from 8% of the volume of the ring. Its mass is about 1 $M_\odot$. The O I recombination radiation may trace a larger fraction of the mass. If it arises in gas like that in model A, it requires a volume of 6×10^{54} cm^3, or 6% of the volume of the ring. Its mass would then be 15 $M_\odot$. However, the cold gas probably produces O I recombination radiation much more efficiently than shown by the models. In weakly ionized plasmas, the electrons ejected by K shell photoionization lose most of their energy by secondary ionizations and excitations, rather than by sharing it with electrons (e.g., Victor and Fox 1988; Shull and Van Steenberg 1985). Assuming 30 eV per ionization about 1 $M_\odot$ of cold, weakly ionized oxygen is sufficient.

e) *Implications for Precursor Star*

The relative abundances in Table 7 may be compared to stellar evolution models such as those of Weaver and Woosley (1980), who calculate models of 15 and 25 $M_\odot$ stars at the point of collapse. The 15 $M_\odot$ model predicts an Ne:O ratio

close to that observed, a C:O ratio about one-half the observed value, and Mg and Si abundances too large by factors of 3. The 25 $M_\odot$ model predicts the observed Mg:O ratio, but Ne:O and Si:O are too low and too high, respectively, by factors of 2 and C:O is too small by a factor of 4. The C:O problem is likely to be aggravated by recent revisions of the $^{12}C(\alpha, \gamma)^{16}O$ rate (cf. Arnettt and Thielemann 1985), so a value closer to the smaller mass is preferable. However, the mass of heavy ($Z \geq 6$) elements ejected in the explosion of a 15 $M_\odot$ star is only 1.24 $M_\odot$ (Woosley and Weaver 1986), which is only marginally consistent with our estimates of the mass of optically emitting gas. This suggests a higher precursor mass. We cannot say at present whether the uncertainties in our mass and abundance determinations or limitations of the supernova models (i.e., spherically symmetric models vs. strongly asymmetric observed ejecta) is the cause of this discrepancy.

It is a pleasure to thank the dedicated staff of the *IUE Observatory* on both sides of the Atlantic for their part in helping procure the ultraviolet data. R. P. Kirshner and P. F. Winkler helped obtain and reduce the CTIO near-IR data, for which we are grateful. Discussion and advice about O I recombination was received from C. W. Bowers and is gratefully acknowledged. This project has been supported by the following grants: NAG 5-701 and NAG 5-988 to the Johns Hopkins University, and NAG 5-87 to the Smithsonian Astrophysical Observatory.

REFERENCES

Arnett, W. D., and Theilemann, F.-K. 1985, *Ap. J.*, **295**, 589.
Blair, W. P., Kirshner, R. P., and Winkler, P. F. 1983, *Ap. J.*, **272**, 84.
Blair, W. P., and Panagia, N. 1987, in *Exploring the Universe with the IUE Satellite*, ed. Y. Kondo (Dordrecht: Reidel), p. 549.
Blair, W. P., Raymond, J. C., Danziger, J., and Matteucci, F. 1988, in *A Decade of UV Astronomy with the IUE Satellite*, ed. Y. Kondo, W. Wamsteker, and R. Wilson (ESA SP-281), p. 117.
Blair, W. P., Raymond, J. C., Fesen, R. A., and Gull, T. R. 1984, *Ap. J.*, **279**, 708.
Boggess, A., *et al.* 1978, *Nature* **275**, 372.
Chevalier, R. A., and Kirshner, R. P. 1978, *Ap. J.*, **219**, 931.
———. 1979, *Ap. J.*, **233**, 154.
Cox, D. P., and Raymond, J. C. 1985, *Ap. J.*, **298**, 651.
Daltabuit, E., and Cox, D. P. 1972, *Ap. J.*, **177**, 855.
Dopita, M. A., Binette, L., and Tuohy, I. R. 1984, *Ap. J.*, **282**, 142 (DBT).
Dopita, M. A., and Tuohy, I. R. 1984, *Ap. J.*, **282**, 135.
Dopita, M. A., Tuohy, I. R., and Mathewson, D. S. 1981, *Ap. J.* (*Letters*), **248**, L105.
Ferland, G. J., Williams, R. E., Lambert, D. L., Schields, G. A., Slovak, M., Gondhalekar, P. M., and Truran, J. W. 1984, *Ap. J.*, **281**, 194.
Fox, J., and Victor, G. S. 1981, *J. Geophys. Res.*, **86**, 2438.
Goss, W. M., Shaver, P. A., Zealey, W. J., Murdin, P., and Clark, D. H. 1979, *M.N.R.A.S.*, **188**, 357.
Gould, R. J. 1978, *Ap. J.*, **219**, 250.
Grandi, S. A. 1980, *Ap. J.*, **238**, 10.
Gronenschild, E. H. J. M., and Mewe, R. 1982, *Astr. Ap. Suppl.*, **48**, 305.
Gull, S. F. 1975, *M.N.R.A.S.*, **171**, 263.
Hamilton, A. J. S., and Fesen, R. A. 1988, *Ap. J.*, **327**, 178.
Hamilton, A. J. S., Sarazin, C. L., and Chevalier, R. A. 1983, *Ap. J. Suppl.*, **51**, 115.
Hartigan, P., Raymond, J., and Hartmann, L. 1987, *Ap. J.*, **316**, 323.
Hughes, J. P., and Helfand, D. J. 1985, *Ap. J.*, **291**, 544.
Hutchings, J. B. 1982, *Ap. J.*, **255**, 70.
Itoh, H. 1977, *Pub. Astr. Soc. Japan*, **29**, 813.
———. 1981, *Pub. Astr. Soc. Japan*, **33**, 1.
———. 1986, *Pub. Astr. Soc. Japan*, **38**, 717.
Julienne, P. S., and Davis, J. 1976, *J. Geophys. Res.*, **81**, 1397.
Julienne, P. S., Davis, J., and Oran, E. 1974, *J. Geophys. Res.*, 79, 2540.
Krolik, J. H., and Kallman, T. R. 1984, *Ap. J.*, **286**, 366.
Lasker, B. 1980, *Ap. J.*, **237**, 765.
Long, K. S., Dopita, M. A., and Tuohy, I. R. 1982, *Ap. J.*, **260**, 202.
Mathewson, D. S., Dopita, M. A., Tuohy, I. R., and Ford, V. L. 1980, *Ap. J.* (*Letters*), **242**, L73.
Mathewson, D. S., Ford, V. L., Dopita, M. A., Tuohy, I. R., Long, K. S., and Helfand, D. J. 1983, *Ap. J. Suppl.*, **51**, 345.
McKee, C. F. 1974, *Ap. J.*, **188**, 335.
McNamara, D. H., and Feltz, K. A. 1980, *Pub. A.S.P.*, **92**, 587.
Murdin, P., and Clark, D. H. 1979, *M.N.R.A.S.*, **189**, 501.
Nandy, K., McLachlan, A., Thompson, G. I., Morgan, D. H., Willis, A. J., Wilson, R., Gondhalekar, P. M., and Houziaux, L. 1982, *M.N.R.A.S.*, **201**, 1P.
Nussbaumer, H., and Storey, P. J. 1983, *Astr. Ap.*, **126**, 75.
———. 1984, *Astr. Ap. Suppl.*, **56**, 293.
Osterbrock, D. E. 1974, *Astrophysics of Gaseous Nebulae* (San Francisco: Freeman).
Prevot, M. L., Lequeux, J., Maurice, E., Prevot, L., and Rocca-Volmerange, B. 1984, *Astr. Ap.*, **132**, 389.
Raymond, J. C., and Smith, B. W. 1977, *Ap. J. Suppl.*, **35**, 419.
Reilman, R. F., and Manson, S. T. 1979, *Ap. J. Suppl.*, **40**, 815.
Rocca-Volmerange, B., Prevot, L., Ferlet, R., Lequeux, J., and Prevot-Burnichon, M. L. 1981, *Astr. Ap.*, **99**, L5.
Seaton, M. J. 1979, *M.N.R.A.S.*, **187**, 79P.
Seward, F. D., and Mitchell, M. 1981, *Ap. J.*, **243**, 736.
Shull, J. M., and Van Steenberg, M. E. 1985, *Ap. J.*, **298**, 268.
Spitzer, L. 1978, *Physical Processes in the Interstellar Medium* (New York: Wiley).
Stone, R. P. S., and Baldwin, J. A. 1983, *M.N.R.A.S.*, **204**, 347.
Strittmatter, P. A., *et al.* 1977, *Ap. J.*, **216**, 23.
Tuohy, I. R., and Dopita, M. A. 1983, *Ap. J.* (*Letters*), **268**, L11.
van den Bergh, S., and Kamper, K. W. 1983, *Ap. J.*, **268**, 129.
Victor, G. S., and Fox, J. 1988, *Planet. Space Sci.*, in press.
Weaver, T. A., and Woosley, S. E. 1980, *Ann. NY Acad. Sci.*, **336**, 335.
Winkler, P. F., and Kirshner, R. P. 1985, *Ap. J.*, **299**, 981.
Woosley, S. E., and Weaver, T. A. 1986, *Ann. Rev. Astr. Ap.*, **24**, 205.

WILLIAM P. BLAIR: Department of Physics and Astronomy, The Johns Hopkins University, Baltimore, MD 21218

JOHN DANZIGER and FRANCESCA MATTEUCCI: European Southern Observatory, Karl Schwartzschild Strasse 2, D-8046 Garching bei München, Federal Republic of Germany

JOHN C. RAYMOND: Harvard-Smithsonian Center for Astrophysics, 60 Garden Street, Cambridge, MA 02138